

# Surveying the Local Supercluster Plane\*

O. G. Kashibadze\*\*,<sup>1</sup> I. D. Karachentsev,<sup>1</sup> and V. E. Karachentseva<sup>2</sup>

<sup>1</sup>*Special Astrophysical Observatory, Russian Academy of Sciences, Nizhnii Arkhyz, 369167 Russia*

<sup>2</sup>*Main Astronomical Observatory, National Academy of Sciences of Ukraine, Kyiv, 03143 Ukraine*

We investigate the distribution and velocity field of galaxies situated in a band of 100 by 20 degrees centered on M87 and oriented along the Local supercluster plane. Our sample amounts 2158 galaxies with radial velocities less than 2000 km s<sup>-1</sup>. Of them, 1119 galaxies (52%) have distance and peculiar velocity estimates. About 3/4 of early-type galaxies are concentrated within the Virgo cluster core, most of the late-type galaxies in the band locate outside the virial radius. Distribution of gas-rich dwarfs with  $M_{\text{HI}} > M_*$  looks to be insensitive to the Virgo cluster presence. Among 50 galaxy groups in the equatorial supercluster band 6 groups have peculiar velocities about 500–1000 km s<sup>-1</sup> comparable with virial motions in rich clusters. The most cryptic case is a flock of nearly 30 galaxies around NGC 4278 (Coma I cloud), moving to us with the mean peculiar velocity of  $-840$  km s<sup>-1</sup>. This cloud (or filament?) resides at a distance of 16.1 Mpc from us and approximately 5 Mpc away from the Virgo center. Galaxies around Virgo cluster exhibit Virgocentric infall with an amplitude of about 500 km s<sup>-1</sup>. Assuming the spherically symmetric radial infall, we estimate the radius of the zero-velocity surface to be  $R_0 = (7.0 \pm 0.3)$  Mpc that yields the total mass of Virgo cluster to be  $(7.4 \pm 0.9) \times 10^{14} M_\odot$  in tight agreement with its virial mass estimates. We conclude that the Virgo outskirts does not contain significant amounts of dark mater beyond its virial core.

Keywords: galaxies: kinematics and dynamics—galaxies: distances and redshifts—galaxies: groups

## INTRODUCTION

The large-scale structure of the Universe—voids, walls, and filaments—evolve through coherent non-Hubble flow motions with amplitude of several hundred km s<sup>-1</sup> on scales of 10–100 Mpc. Such a pattern is resulting from N-body simulations in the standard cosmological  $\Lambda$ CDM model [1–3]. Actually, the Milky Way, together with dozens of other neighboring galaxies forming the planar structure of the *Local Sheet*, moves relative to the cosmic microwave background with a velocity of 630 km s<sup>-1</sup> [4]. According to Tully et al. [5, 6], this velocity vector is composed of three roughly orthogonal components: (1) infall of the Local Sheet toward the center of the nearest Virgo cluster with a velocity of 185 km s<sup>-1</sup>, (2) outflow from the expanding

Local Void with the velocity of 260 km s<sup>-1</sup> and (3) bulk motion toward Hydra–Centaurus cluster and the Shapley supercluster [7] with an amplitude of about 450 km s<sup>-1</sup>. This complicated background of multidirectional flows makes it useless to estimate distances of nearby galaxies via the linear Hubble relation:  $V_{\text{LG}} = H_0 D$ , where  $D$  is distance of a neighboring galaxy,  $V_{\text{LG}}$  is its radial velocity relative to the Local Group centroid and  $H_0$  is the Hubble parameter. Even those models of non-Hubble velocity fields which consider only the Virgo cluster but not other components [8, 9] are yet too simplified to determine distances of Local Supercluster (LSC) galaxies from their radial velocities.

Large-area sky surveys in neutral hydrogen (HI) 21-centimeter line—HIPASS [10], ALFALFA [11], WSRT-CVn [12]—gave an opportunity of the wholesale measurements of distances to galaxies with an accuracy of approximately 20–25% from Tully–Fisher [13] relation between the luminosity of a galaxy and the width of its HI line. At this stage the Tully–Fisher distance estimates are made for several thousand galaxies

\* Table I is available at the CDS via anonymous ftp <ftp://cdsarc.u-strasbg.fr/pub/cats/J/other/AstBu/73.124> (130.79.128.5) or via <http://vizier.u-strasbg.fr/viz-bin/VizieR?source=J/other/AstBu/73.124>

\*\*phiruzi@gmail.com

with typical velocities of about  $6000 \text{ km s}^{-1}$  [6], making the basis for studying cosmic flows in the scale of about 100–200 Mpc.

Inside the Local Supercluster ( $D < 30 \text{ Mpc}$ ) with the Virgo cluster located at 16.7 Mpc [14] as its core, there are many spiral and irregular galaxies with measured HI line widths  $W_{50}$  but without distance estimates. For many of them we determined Tully–Fisher distances for the first time, increasing the density of the peculiar velocity field in the Local Supercluster more than twice.

In our previous papers we considered motions of galaxies in several regions along the LSC equator: Coma I [15], Ursa Major [16], Virgo Southern Extension [17], as well as in broad bands Leo–Cancer [18], Bootes [19] and Hercules–Bootes [20] flanking to the LSC equator. In the last cases, we have obtained new evidence that the Local Void expands, while galaxies in the vicinity of the Virgo cluster move toward its center. Beyond that, we had considered particularly the kinematic situation around the Virgo and Fornax clusters and the Local Void [21–23] and estimated the total mass for both clusters, as well as the density contrast in the Local Void. The map with the discussed areas distributed over the sky in equatorial coordinates is shown in Fig. 1 where dots mark 5180 galaxies with radial velocities  $V_{LG} < 2000 \text{ km s}^{-1}$  and the floccose annular band represents the Zone of Avoidance obscured by the Milky Way.

### SAMPLE OF GALAXIES IN THE LSC PLANE

We used HyperLEDA<sup>1</sup> [24] and NASA Extragalactic Database (NED)<sup>2</sup> as the main sources of observational data on LSC galaxies amplifying them by the most recent estimates of galaxy distances. We have selected galaxies in the band  $\pm 10^\circ$  by the supergalactic latitude (SGB) and  $\pm 50^\circ$  by the supergalactic longitude (SGL) relative to the Virgo cluster center which has

been identified with the radio galaxy M87 = NGC 4486 (SGL =  $102^\circ 88$ , SGB =  $-2^\circ 35$ ). The reason for such a choice is that M87 is situated near the barycenter of the hot X-ray emitting intracluster gas. We have filtered our sample by radial velocities relative to the Local Group centroid, keeping only galaxies with  $V_{LG} < 2000 \text{ km s}^{-1}$ . This condition allows to cover the essential population of the Virgo cluster and the adjacent structures avoiding a large number of distant background galaxies<sup>3</sup>.

Totally, 3995 objects from HyperLEDA and NED databases satisfy these conditions. We have investigated visually all object images in the Digital Sky Survey (DSS), Sloan Digital Sky Survey (SDSS) [26] and Panoramic Survey Telescope and Rapid Response System (PanSTARRS) [27] verifying and refining galaxy morphological classification. As a result, we have excluded 1837 fake objects from this sample; all of them turned out to be stars projected onto distant galaxies, different parts of one and the same galaxy, or ambiguous optical identifications of radio sources. It is worth accentuating that the noncritical, formal use of basic data should lead to about 46% of “spam” in the reviewed sample, corrupting the further analysis.

We have obtained new distance estimates for 563 galaxies from this list. 386 estimates have been resulted from the relation of Tully and Pierce [28]:

$$M_B = 7.27(2.5 - \log W_{50}) - 19.99;$$

the hydrogen line widths are corrected for galaxy inclinations, and the data on axial ratio have been extracted from HyperLEDA. Distance estimates for the remaining 177 gas-rich dwarf galaxies have been derived from the baryonic Tully–Fisher relation [29]. The authors have argued that considering inclinations of dwarf galaxies does not noticeably improve the dispersion on the Tully–Fisher diagram. For that reason, we have not applied corrections for galaxy inclinations in the case of baryonic TF-relation.

The resulting list of 2158 galaxies is presented in Table I with the full machine readable version

<sup>1</sup> <http://leda.univ-lyon1.fr/>

<sup>2</sup> <http://ned.ipac.caltech.edu/>

<sup>3</sup> We have changed this limit up to  $2600 \text{ km s}^{-1}$  for the upcoming analysis of the virial zone itself [25].

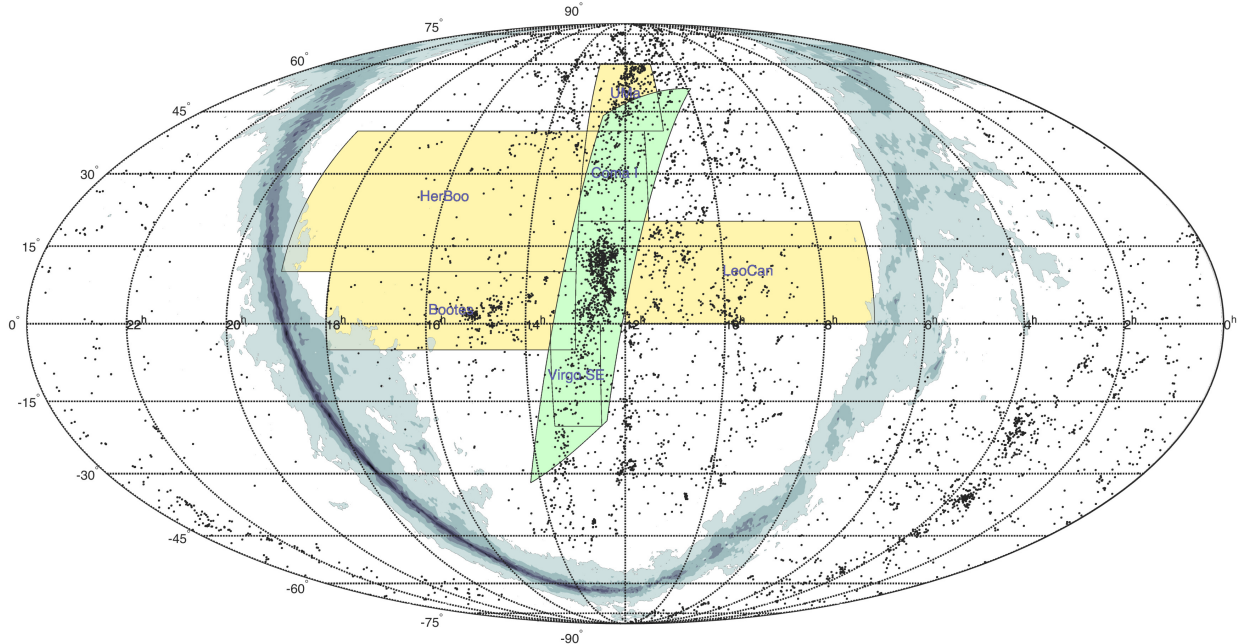


FIG. 1. The distribution of 5180 galaxies with radial velocities  $V_{LG} < 2000 \text{ km s}^{-1}$  over the sky in equatorial coordinates. The Zone of Avoidance near the plane of the Milky Way is shadowed. The region being considered in this paper is filled with green. Other sky areas discussed before are marked by yellow. (See electronic version of the paper for colored figures.)

available at SIMBAD Astronomical Database<sup>4</sup>. The table columns contain (1) galaxy name; (2) equatorial coordinates J2000.0; (3) supergalactic coordinates; (4) radial velocity of a galaxy ( $\text{km s}^{-1}$ ) relative to the Local Group centroid with apex parameters adopted in NED; (5) morphological type according to de Vaucouleurs classification; in addition to the de Vaucouleurs types we note also for compact objects: Ec (compact ellipticals) and BCD (blue compact dwarfs); for dwarfs of low and very low surface brightness we use the designations: Ed, Edn (elliptical shape), Sph, Sphn (round); the symbol “n” means a presence of a star-like nucleus; I, Ir (diffuse objects having no blue knots); (6) apparent  $B$ -magnitude from HyperLEDA or NED, values without decimals indicate our visual estimates; (7) 21-cm HI line width ( $\text{km s}^{-1}$ ) at half maximum; (8) apparent HI-magnitude  $m_{21} = 17.4 - 2.5 \log F(\text{HI})$ , where  $F(\text{HI})$  is the HI line flow ( $\text{Jy km s}^{-1}$ ); (9), (10) distance modulus and galaxy distance (Mpc);

(11) method applied to determine distance. We distinguished methods based on supernovae (SN) and cepheids (cep) luminosity, the tip of the red giant branch (rgb) recipe [30], and the surface brightness fluctuation (sbf) method [31]. The distance estimates made by these techniques have an accuracy of 5–10%, and we specify them as “accurate” hereafter. The secondary or “supplement” distance estimates—from the Tully–Fisher relation (TF or tf), the fundamental plane (FP) or from globular cluster luminosity (gc), calibrated by cepheids, have a typical accuracy of 20–25%. We have marked Tully–Fisher distances extracted from NED as “tf”, while our new estimates after Tully and Pierce [28] are denoted with capitals “TF”; in the case of gas-rich dwarf galaxies their distances after Karachentsev et al. [29] are labeled as “TFb”. In total, galaxies with distance measurements amount to 1119, which is 52% of the total sample. The catalog Cosmicflows-3 Distances [6] contains only 450 distance estimates in this region.

<sup>4</sup> <http://vizier.u-strasbg.fr/viz-bin/VizieR?source=J/other/AstBu/73.124>

The distribution of galaxies by their supergalactic coordinates is presented in Fig. 2, where

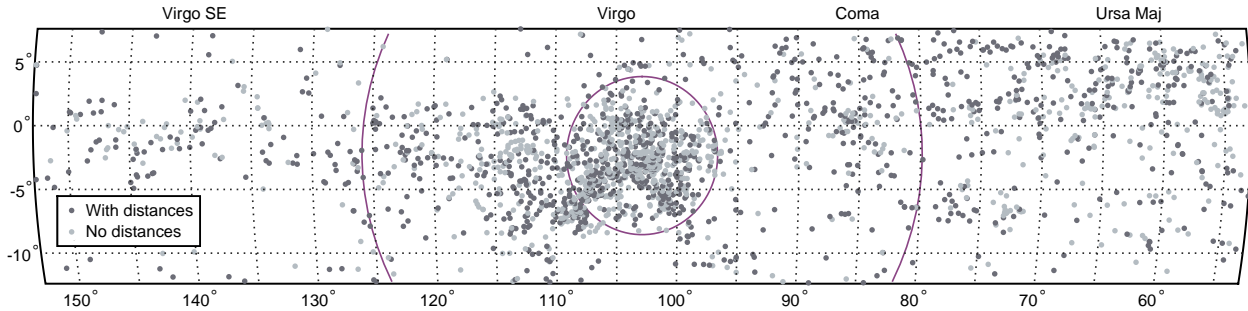


FIG. 2. Distribution of 2158 galaxies of the LSC belt with radial velocities  $V_{\text{LG}} < 2000 \text{ km s}^{-1}$  over the sky in supergalactic coordinates. Galaxies with distance estimates are marked by darker symbols. The central circle and the arcs denote the virial radius (1.8 Mpc) and the radius of the zero velocity surface (7.2 Mpc) for the Virgo cluster.

objects with measured distances and without them are shown with dark and open markers, respectively. The central circle with the radius of  $6^{\circ}2$  outlines the virial zone of the Virgo cluster (the virial radius  $R_V = 1.8 \text{ Mpc}$ ), and the arcs of the bigger circle  $23^{\circ}6$  or  $R_0 = 7.2 \text{ Mpc}$  separate the infall region from the cosmological expansion. As it can be seen, the distribution of galaxies outside the virial zone is notably non-uniform and asymmetric, while the ratio of galaxies with measured distances does not change significantly from the left (southern) side of the belt to the right (northern) one. All three dynamical zones: the virial core, the infall zone and the field are well represented in our sample.

Figure 3 shows the distribution of LSC belt galaxies by their distances measured from different methods. Three top panels correspond to highly accurate methods. 80 galaxies with RGB distances are supplemented by 12 galaxies with distances measured from their obvious membership (mem) in groups with reliable distance estimates of other members, generally more bright. Three bottom panels of Fig. 3 depict the distribution of galaxies with less accurate distances. Comparison of these data demonstrates the inherent difference between the applied methods in their effective depth: galaxies with RGB distances are concentrated mainly in the Local Volume ( $D < 11 \text{ Mpc}$ ) while the bulk of galaxies with Tully–Fisher distances resides behind the Virgo cluster. The peak  $N(D)$  values at  $D \simeq 16 \text{ Mpc}$  are caused by the Virgo cluster members. However, gas-rich dwarfs with “TFb”

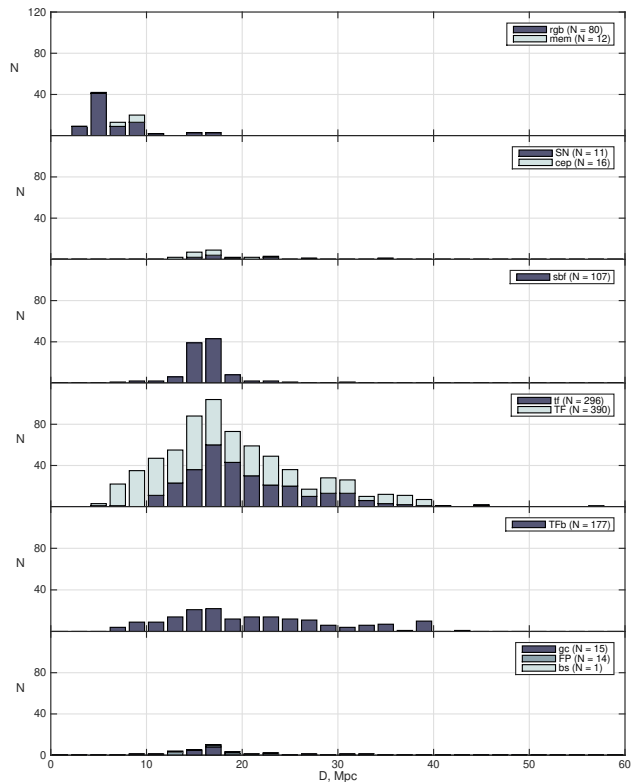


FIG. 3. Distribution of the LSC galaxies by distances measured from different methods.

distances do not show such a peak. These factors should be considered when analyzing the infall of galaxies toward the Virgo center from foreground and background of the cluster.

The general distribution of LSC belt galaxies by their radial velocities, distances and peculiar velocities  $V_{\text{pec}} = V_{\text{LG}} - H_0 D$ , where  $H_0 = 73 \text{ km s}^{-1} \text{ Mpc}^{-1}$ , is presented in three panels of Fig. 4. The wide peak  $N(V_{\text{LG}})$  with

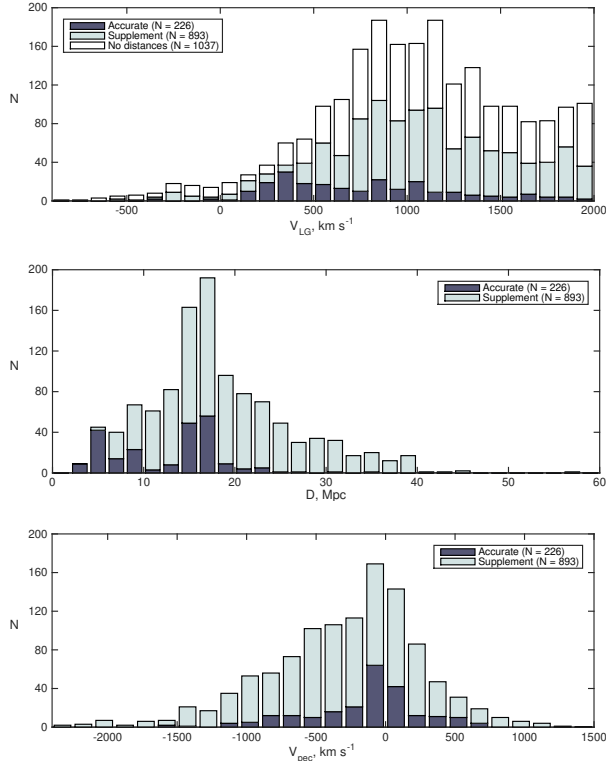


FIG. 4. Distribution of the LSC galaxies by (top) radial velocities, (middle) distances and (bottom) peculiar velocities. Galaxies with accurate distances are marked with dark grey.

$V_{LG} = 1000 \pm 500 \text{ km s}^{-1}$  is formed by members of the Virgo cluster and the adjacent structures. The ratio of galaxies without distance estimates grows faintly with radial velocities. As it can be seen from the middle panel data, more than 99% of galaxies have distances within 40 Mpc. The tail area of distribution ( $D = 40\text{--}60$  Mpc) might be due to systematical errors in measured widths  $W_{50}$ , like in the case of UGC 6372.

Peculiar velocities of galaxies are distributed in the wide range of  $[-2300, +1300] \text{ km s}^{-1}$  with the maximum near zero. The  $N(V_{pec})$  histogram looks asymmetric and shifted to negative values  $V_{pec}$ . The observed asymmetry could have different reasons, such as:

- (a) the motion of the Local Group toward the Virgo center with the velocity of about  $200 \text{ km s}^{-1}$ ;
- (b) the limit of  $V_{LG} < 2000 \text{ km s}^{-1}$  filtering out a part of falling galaxies at the foreground side of the cluster but passing ones that are moving

from the background side;

(c) the Malmquist bias manifesting itself when symmetrical errors of distance moduli  $\Delta(m - M)$  turn into asymmetrical errors of distances  $\Delta D$  (this effect is less noticeable for galaxies with accurate distance estimates);

(d) the galaxy associations with significant peculiar velocities presenting in the LSC belt; in such a case the large positive peculiar velocities are cut off by the condition  $V_{LG} < 2000 \text{ km s}^{-1}$  while the conspicuous negative peculiar velocities satisfy this condition.

## OBSERVING TRENDS ALONG SGL

### Kinematic/Geometric Trends

In the standard cosmological model  $\Lambda$ CDM galaxy clusters are formed as dense hub at the crossing of walls and filaments; along these structures, galaxies fall into the virial zone of a cluster. The distribution of galaxies by their distances and radial velocities should have been impacted by galaxy flows along cosmic filaments. Tully et al. [6] suggested that the main channel feeding the virial zone of the Virgo cluster is the Virgo Southern Extension filament (VirgoSE) at supergalactic latitudes  $SGL > 110^\circ$ . Figures 5 and 6 show the distribution of velocities and distances of galaxies along SGL. Taking into account the selection effects listed above, we have divided the LSC belt galaxies into two subsamples having accurate and secondary distance indicators. The bold line reflects the running median with smoothing window of  $\Delta SGL = 4^\circ$ , and narrow lines above and below correspond to running quartiles.

As it can be seen, in the case of “accurate” distances (top panels of Figs. 5 and 6) the median velocity and the median distance tend to increase from the belt ends to its center fixed by the Virgo cluster. This is just what should be expected if galaxies move along the southern and northern filaments adjoining the Virgo cluster by their far ends. However, this phenomenon could also be caused by the selection effect: Ferrarese et al. [32] and Mei et al. [14] carried out

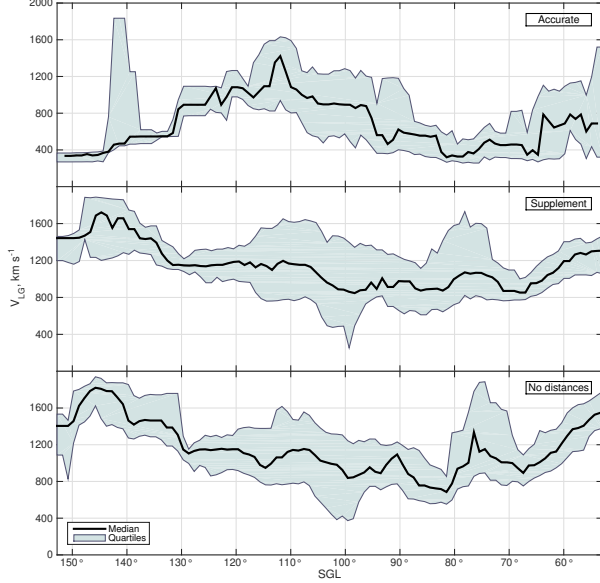


FIG. 5. Running median and quartiles of radial velocities along the LSC belt for galaxies with measured (top, middle) and unknown (bottom) distances.

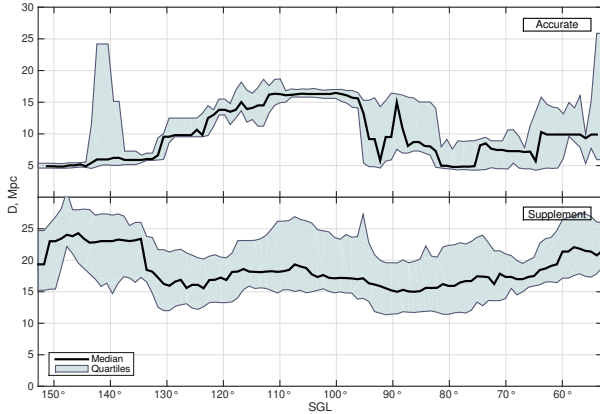


FIG. 6. Running median and quartiles of distances along the supergalactic longitude.

special efforts to measure distances of galaxies in the Virgo core by RGB and SBF methods, while at the ends of the belt RGB distances are available only for members of the nearest groups (NGC 4244, NGC 4631, NGC 5236). Another pattern is demonstrated by the running median in the case of TF distances (middle panel of Fig. 5). Note also that the drift of  $V_{LG}$  running median for galaxies without distance estimates (bottom panel of Fig. 5) repeats roughly the shape of the median in the middle panel.

As it follows from the data presented at the top panel of Fig. 6, the scatter of accurate distances in the virial zone of the cluster ( $SGL = 97 - 110^\circ$ ) is remarkably small and comparable with the virial radius of the cluster. The band-average interquartile width for accurate distances is 2 or 3 times less than the similar width for supplement distances, corresponding roughly to the accuracy ratio for these methods (5–10% vs. 20–25%).

Figure 7 shows the running median and quartiles for peculiar velocities of galaxies along supergalactic longitude. At the ends of the belt  $SGL < 80^\circ$  and  $SGL > 130^\circ$  galaxies with accurate distances demonstrate insignificant shift and small scatter of peculiar velocities. This is caused by the fact that most of them belongs to the “cold” Local Sheet where the random non-Hubble velocities are minor. On the contrary, galaxies with TF distances are situated mainly at the far end of the volume external to the Local Sheet, having predominantly negative peculiar velocities. Both subsamples in the top and bottom panels detect the predicted growth of  $V_{pec}$  dispersion in the center of the belt due to the virial motions in the cluster.

Another feature being seen in the top panel of Fig. 7 is the excess of galaxies with positive peculiar velocities near the southern side of the Virgo cluster ( $SGL \simeq 113^\circ$ ). It is probably caused by the association of galaxies around NGC 4527 situated at the proximal side of the Virgo cluster and falling toward its center. Yet another

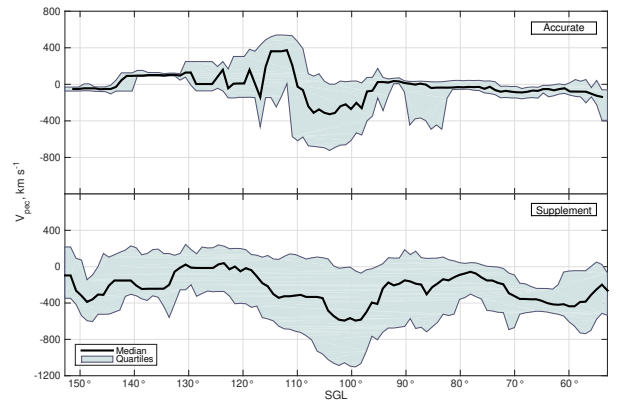


FIG. 7. Running median and quartiles of peculiar velocities along the LSC belt.

feature—the zone of negative values of  $V_{\text{pec}}$ —can be seen in the interval of  $\text{SGL} = 83^\circ\text{--}90^\circ$ . It corresponds to the velocity anomaly in Coma I [15] and will be discussed in more detail below.

As it follows from the data presented at both panels of Fig. 7, the general trend of the median peculiar velocity along the belt is imperceptible as expected in the case when filamentary structures near the Virgo cluster are oriented almost perpendicular to the line of sight.

### Morphological Landscape

The distribution of LSC belt galaxies by their morphological types is shown in Fig. 8; the radial velocity or distance scales are given below each panel. The early type galaxies demonstrate strong concentration toward the core of the Virgo cluster (top panel of Fig. 8). About 3/4 of them are located inside the virial radius of the cluster, and the others are associated with galaxy groups. The equatorial group with  $\text{SGL} \simeq 86^\circ$  corresponds to the Coma I cloud around NGC 4278 with significant negative peculiar velocities.

The distribution of the late type galaxies in the middle panel shows much lesser concentration toward the virial zone of the Virgo cluster. This effect is well known as morphological segregation reflecting the density of the environment.

Haynes and Giovanelli [33] have pointed out that spiral galaxies of a certain morphological type located in the Virgo cluster core are characterized with HI deficiency relative to the field galaxies of the same type. Ram pressure stripping of gas in the dense virial zone of the cluster is the evident scheme explaining the HI deficiency.<sup>5</sup> The stripping process is most effective for irregular dwarf galaxies because of their shallow potential wells. The bottom panel of Fig. 8 represents the distribution of the gas-rich dwarfs ( $m_{21} < B_T$ ) with baryonic Tully–Fisher distances. The concentration of these objects

toward the Virgo cluster is hardly detectable providing a detached perspective of the HI deficiency phenomenon. Some lack of uniformity in the distribution of gas-rich galaxies over the considered region is caused by the borders of the HIPASS and ALFALFA HI surveys.

### Nearby Groups in the LSC Band

Makarov and Karachentsev [35] (MK 11) have published a list of 350 groups consisting of galaxies with radial velocities  $V_{\text{LG}} < 3500 \text{ km s}^{-1}$ . This all-sky sample includes 50 groups with coordinates falling into the LSC belt and having mean radial velocity  $V_{\text{LG}} < 2000 \text{ km s}^{-1}$ . These groups are listed in Table II. Its columns contains (1) name of the brightest member; (2), (3) supergalactic coordinates of the group center; (4) number of galaxies with measured radial velocities; (5) mean radial velocity of a group ( $\text{km s}^{-1}$ ); (6) mean group distance (Mpc); (7) peculiar velocity of a group ( $\text{km s}^{-1}$ ).

It should be noted that MK 11 galaxy clustering criterion used velocity based distance estimates, as there were only few direct distance measurements at that time. This circumstance has caused some uncertainty in clustering results for the Virgo virial zone characterized by large motions. The bulk of Virgo galaxies has been clustered around giant elliptical NGC 4472 instead of NGC 4486. Moreover, several galaxy groups with small radial velocities (NGC 4216, NGC 4342, NGC 4402, NGC 4552) turned out to be fake structures.

Figure 9 shows the distribution of 50 MK 11 groups marked as circles over the considered region. The size of a circle is proportional to logarithmic number of galaxies with measured radial velocities, and the color reflects mean radial velocity of a group according to the scale given below.

As it follows from the data presented in the last column of Table II, some galaxy groups have significant peculiar velocities  $|V_{\text{pec}}| > 500 \text{ km s}^{-1}$ :  $-749 \text{ km s}^{-1}$  (NGC 3838),  $-518 \text{ km s}^{-1}$  (NGC 3900),  $-972 \text{ km s}^{-1}$  (NGC 4150),  $+534 \text{ km s}^{-1}$  (NGC 4527),  $-542 \text{ km s}^{-1}$  (NGC 4636),  $-754 \text{ km s}^{-1}$

<sup>5</sup> Planck Collaboration [34] have reported on detection of the Sunyaev–Zeldovich effect from the Virgo cluster. They estimate the mass of the hot intracluster gas as  $(1.5 \pm 0.1) \times 10^{14} M_\odot$ , which is 17 (!) times more than the total stellar mass of the cluster.

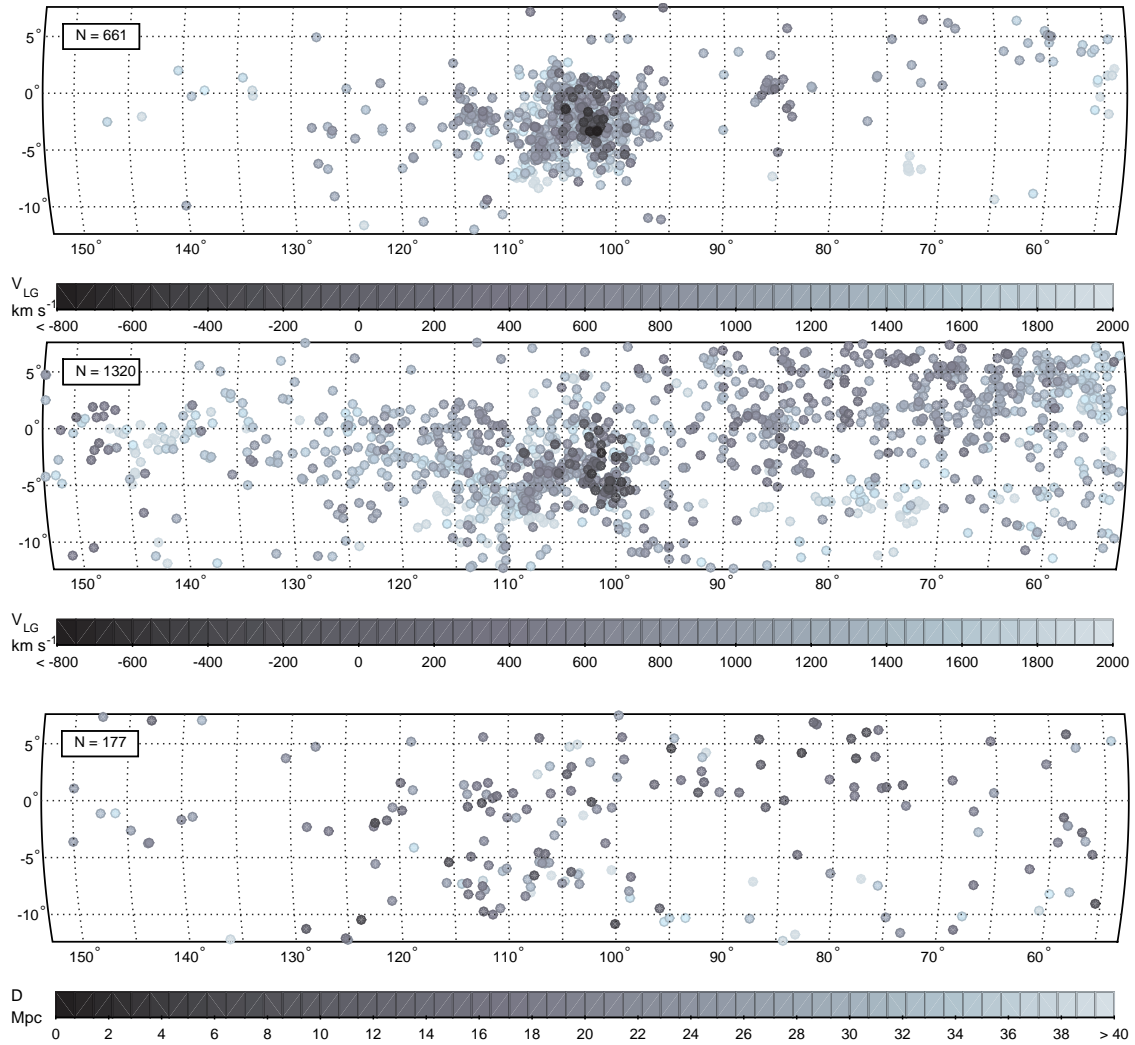


FIG. 8. Distribution of (top) early type galaxies, (middle) late type galaxies, (bottom) gas-rich dwarfs along the LSC belt. Radial velocity or distance scales are given below each panel.

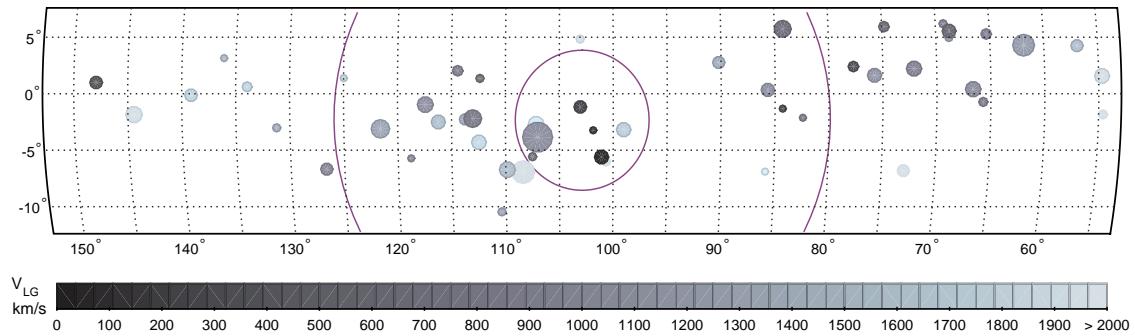


FIG. 9. Galaxy groups in the considered region. The marker size is proportional to logarithmic number of galaxies with measured radial velocities; the density specifies mean radial velocity of a group according to the scale given below. The large and small circles correspond to the radius of the zero velocity surface and the virial radius of the Virgo cluster.



(NGC 4900). If the individual distance error is equal to approximately 20% and the group includes more than four members with distance estimates, then the expected peculiar velocity error makes less than  $150 \text{ km s}^{-1}$  for the typical distance of nearly 20 Mpc. Hence, the conspicuous peculiar velocities of several groups in the vicinity of Virgo have physical origins and do not result from errors in distance measurements.

### VELOCITY ANOMALY IN COMA I

The most spectacular example of significant peculiar velocities is the galaxy association near NGC 4278 known as Coma I cloud. Considering probable Local Volume galaxies with velocities  $V_{\text{LG}} < 600 \text{ km s}^{-1}$ , Karachentsev et al. [15] have noticed that the most distant ones ( $D > 13 \text{ Mpc}$ ) cover the sky in quite a spotty manner. New data originating from ALFALFA HI survey make this pattern even more contrast.

The distribution of galaxies with  $V_{\text{LG}} < 600 \text{ km s}^{-1}$  and  $D > 13 \text{ Mpc}$  over the LSC belt is presented in the top panel of Fig. 10. Galaxies with accurate and less precise distances are depicted, respectively, as circles and asterisks. Predictably, the center of this image is filled with Virgo members having large virial velocities directed toward the observer. Besides the Virgo cluster, the diagram displays the only structure appearing as a galaxy cloud around the massive elliptical galaxy NGC 4278 near  $\text{SGL} = 86^\circ$  and  $\text{SGB} = 0^\circ$ . The probability of all 23 galaxies outside the Virgo core laying rightward does not exceed  $10^{-6}$ .

We have considered the wide outskirts of NGC 4278 and distinguished 28 distant galaxies with small radial velocities as possible members of the Coma I cloud. We have enlarged this sample with other ten galaxies which have not yet distance estimates but can still belong to this cloud, by reference to their texture. The whole sample is presented in the Table III. Its columns contain (1) galaxy name; (2) equatorial coordinates; (3) de Vaucouleurs numerical morphological type; (4) radial velocity ( $\text{km s}^{-1}$ ); (5), (6) galaxy distance (Mpc) and the method applied to determine it; (7) apparent

$B$ -magnitude; (8) peculiar velocity ( $\text{km s}^{-1}$ ). The distribution of these galaxies is shown in the bottom panel of Fig. 10. Galaxies with measured distances are marked solid while galaxies without distance estimates are represented as open markers. Small and large circles specify the virial radius (270 kpc) and the radius of the zero-velocity surface (1.0 Mpc) around the NGC 4278 taking its distance to be 16.1 Mpc.

As one can see, the Coma I cloud is a rather loose formation with only 1/3 of the galaxies inside the virial radius. On the other hand, the presence of early type galaxies ( $T < 0$ ) in the Coma I cloud indicate the later stage of the group evolution. Probably, NGC 4278 with its satellites forms a part of an elongated filament or sheet with the mean peculiar velocity of  $-840 \text{ km s}^{-1}$ , which is comparable with virial velocities in rich galaxy clusters.

The Coma I cloud is situated at the angular distance of about  $18^\circ$  from the Virgo center, i.e. near the radius of its zero-velocity surface ( $23^\circ$ ). The distances of both structures are roughly equal: 16.1 Mpc and 16.7 Mpc. Thus, the expected radial infall of the Coma I cloud to the Virgo cluster supposes its motion to be close to tangential. In this case the Coma I peculiar velocity should be insignificant.

Earlier we have made a suggestion [15] that conspicuous peculiar motions in the Coma I region could be associated with a dark attractor having mass of about  $2 \times 10^{14} M_\odot$ . Another explanation of this puzzling phenomenon assumes a fast coherent motion of the whole filament with the NGC 4278 group toward the observer. But the source of such a high velocity stays unclear. Note, however, that the mean peculiar velocity of the Coma I cloud in the cosmic microwave background (CMB) reference frame appears to be appreciably lower ( $-526 \text{ km s}^{-1}$ ) as compared to its peculiar velocity in the Local Group reference frame ( $-840 \text{ km s}^{-1}$ ).

### VIRGOCENTRIC INFALL

The neighboring massive Virgo cluster produces significant distortions in the velocity field of nearby galaxies relative to the undisturbed

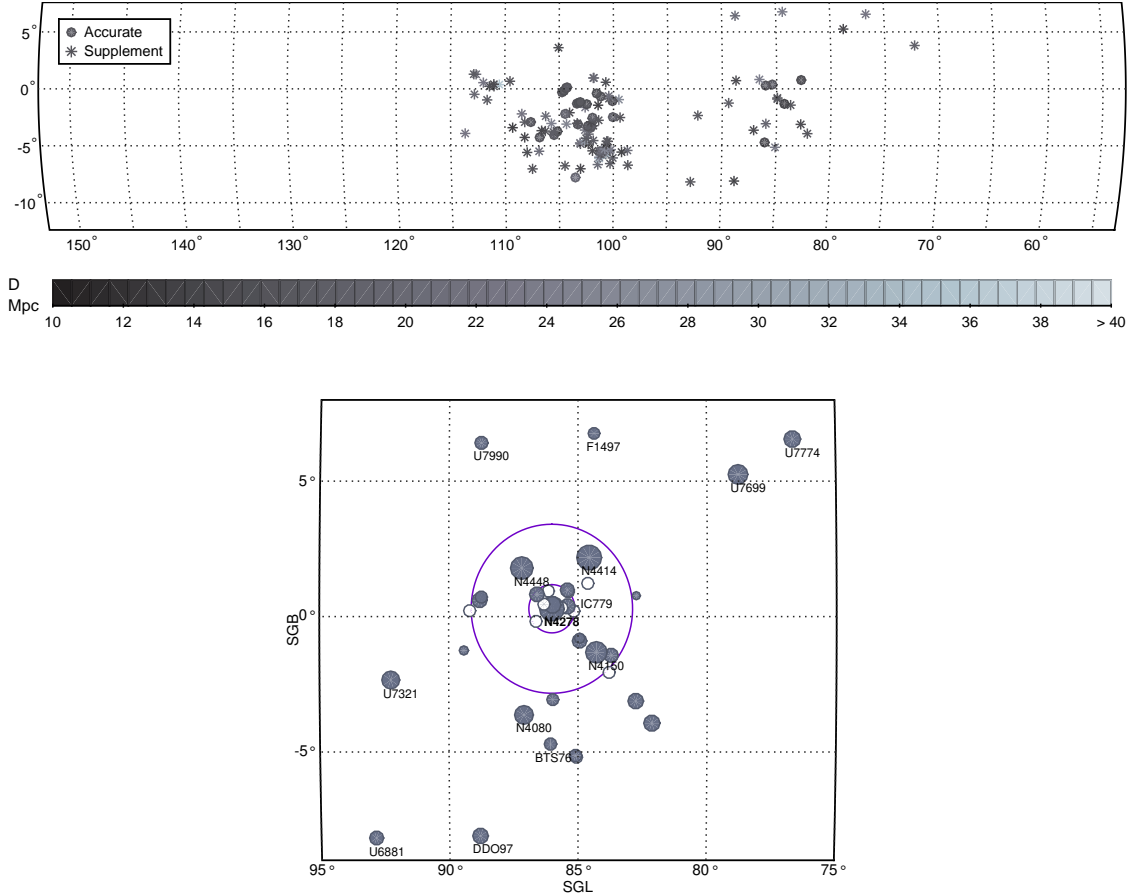


FIG. 10. Distribution of LSC belt galaxies with distances  $D > 13$  Mpc and radial velocities  $V_{LG} < 600$  km s $^{-1}$  (top panel). Galaxies with “accurate” and “supplement” distances are marked by circles and asterisks, respectively. Bottom panel: distribution of Coma I cloud galaxies around NGC 4278 in supergalactic coordinates. The marker size is proportional to logarithmic stellar mass of a galaxy. Open circles denote galaxies without individual distance estimates.

Hubble flow. The dynamical models and the observational evidences of this effect known as Virgocentric infall were studied by Hoffman et al. [36], Tonry and Davis [37], Hoffman and Salpeter [38], Tully and Shaya [39], Teerikorpi et al. [40], Ekholm et al. [41], Tonry et al. [31, 42], and Karachentsev and Nasonova [21]. Using the highly accurate Hubble Space Telescope distance measurements for galaxies located near the proximal side of the Virgo cluster, Karachentsev et al. [43] have determined the radius of the zero-velocity surface separating the infall region from the global cosmic expansion to be  $R_0 = 7.2 \pm 0.7$  Mpc. The total mass of the cluster inside the  $R_0$  radius is expressed as

$$M_T = (\pi^2/8G)R_0^3 H_0^2 / f^2(\Omega_m),$$

where the dimensionless parameter

$$f(\Omega_m) = (1 - \Omega_m)^{-1} - \frac{\Omega_m}{2}(1 - \Omega_m)^{-\frac{3}{2}} \cosh^{-1}\left(\frac{2}{\Omega_m} - 1\right)$$

changes in the range from 1 to 2/3 while varying  $\Omega_m$  from 0 to 1. In the standard cosmological model with  $\Omega_m = 0.24$  and  $H_0 = 73$  km s $^{-1}$  Mpc $^{-1}$ , it corresponds to the total mass of the cluster  $M_T = (8.3 \pm 2.3) \times 10^{14} M_\odot$  matching closely the virial mass estimates:  $6.2 \times 10^{14} M_\odot$  [44],  $7.5 \times 10^{14} M_\odot$  [39] and  $7.2 \times 10^{14} M_\odot$  [45].

The new data on distances of galaxies situated along the Local Supercluster equator give the reason to reestimate  $R_0$  and  $M_T$  parameters for the Virgo cluster. Figure 11 presents

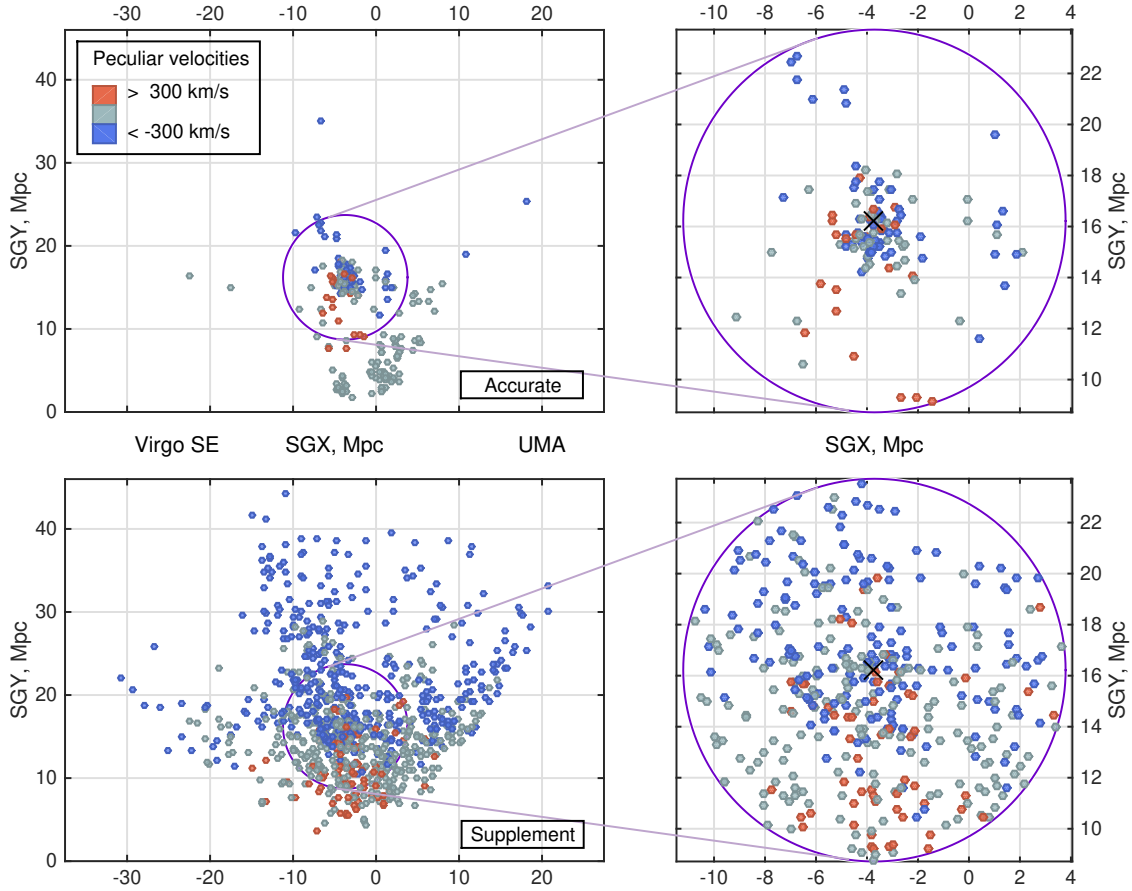


FIG. 11. Distribution of galaxies with large and small peculiar velocities in Cartesian supergalactic coordinates. The circle corresponds to the radius of the zero velocity surface.

the distribution of the LSC belt galaxies projected onto the Local Supercluster plane in Cartesian supergalactic coordinates. The top and the bottom panels correspond to the “accurate” and “supplement” subsamples. The galaxy landscape inside the  $R_0$  radius is inset rightward. Red and blue markers indicate galaxies with peculiar velocities  $V_{\text{pec}} < -300 \text{ km s}^{-1}$  and  $V_{\text{pec}} > +300 \text{ km s}^{-1}$ , respectively. Galaxies with insignificant (intermediate) peculiar velocities are marked with grey.

The spherical infall pattern supposes nearby galaxies with positive peculiar velocities to be situated at the foreground side of the Virgo cluster while galaxies having negative peculiar velocities should lie at its distant side. Such an effect is actually observed in Fig. 11 for both subsamples. Several galaxies in the bottom panel deviate from this regularity since the typical error for their Tully–Fisher distances is 3–4 Mpc, be-

ing comparable with the virial diameter of the Virgo cluster (3.6 Mpc).

“Grey” galaxies with  $|V_{\text{pec}}| < 300 \text{ km s}^{-1}$  in the top panel form the Local Sheet elongated in the direction of Ursa Major. The size of this “cold” domain amounts to about  $5 \times 15 \text{ Mpc}$ . The bottom, more populated panel manifests some signs of an empty sector behind the Virgo cluster spreading toward the Virgo Southern Extension. The data presented in the Table I are obviously insufficient to detect the distant side of this void.

The overrepresentation of galaxies with negative peculiar velocities in the Fig. 11 is caused both by infall of the Local Sheet toward the Virgo cluster with the velocity of approximately  $200 \text{ km s}^{-1}$  and by bulk motion of galaxies behind the cluster toward its center, i.e. in the direction of the observer.

To estimate the radius  $R_0$  of the zero veloc-

ity surface, we have calculated virgocentric distances of galaxies

$$D_{\text{vc}}^2 = D_g^2 + D_c^2 - 2D_g D_c \cos \Theta, \quad (1)$$

where  $D_g$  and  $D_c$  are the distances from the observer to a galaxy and to the Virgo center respectively, and  $\Theta$  is the angular distance of a galaxy from the Virgo center. The velocity of a galaxy relative to the cluster center has been defined within the “minor attractor” model:

$$V_{\text{vc}} = V_g \cos \lambda - V_c \cos(\lambda + \Theta), \quad (2)$$

where  $\lambda$  is the angle between the line of sight and the direction from the cluster center to a galaxy:  $\tan \lambda = D_c \sin \Theta / (D_g - D_c \cos \Theta)$ , or within the “major attractor” model

$$V_{\text{vc}} = [V_c \cos \Theta - V_g] / \cos \lambda. \quad (3)$$

The first case supposes that the peculiar velocities of galaxies are small compared to the regular Hubble flow. The second case implies that the infall velocity predominates for most galaxies (see details in [21]). The difference between two models becomes insignificant if a galaxy is located strictly behind  $\lambda \simeq 0$  or in front of  $\lambda \simeq 180^\circ$  the cluster center.

For relating  $V_{\text{vc}}$  to  $D_{\text{vc}}$  it is essential to fix both the distance and the radial velocity of the Virgo center. According to Mei et al. [14],  $D_c = 16.7 \pm 0.2$  Mpc.

Fixing  $V_c$  is a more complicated problem. The mean radial velocity and the radial velocity dispersion are known to depend on the morphological composition of the sample [46]. Since different methods of distance measurements use morphologically diverse samples, and because of the morphological segregation in the cluster, various  $V_c$  estimation approaches suffer severely from inconsistency. Additional complications appear due to the presence of substructures forming the Virgo cluster: M87 cluster, M49 cluster, being projected onto the more distant structures: W cloud, M cloud, NGC 4636 group [47, 48].

A modest summary of  $V_c$  estimates known from literature is presented in the upper part of the Table IV. Some its values are estimated only for the Virgo core while others correspond

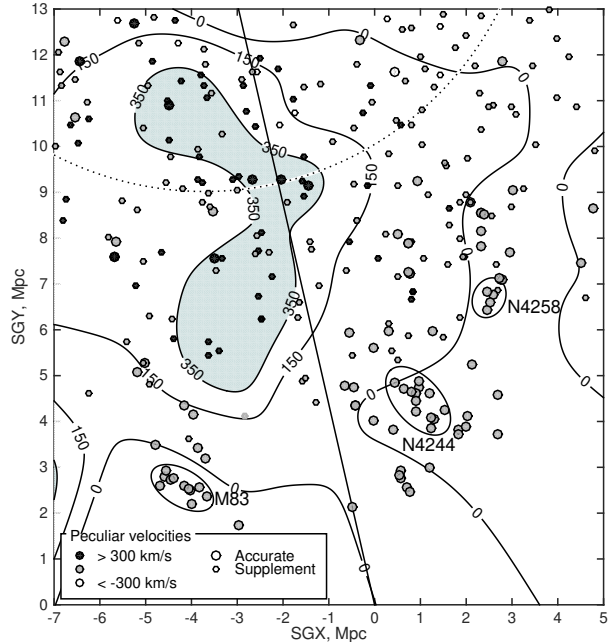


FIG. 12. Peculiar velocity field at the proximal side of the Virgo cluster.

to the whole cluster. The number of galaxies in individual samples differ by an order. Binggeli et al. [46] have used only radial velocity data, while Mei et al. [14] have taken into account their own distance estimates. Two cases ([5, 31]) derive the peculiar velocity of the Virgo cluster  $V_{c, \text{pec}} = V_c - 73D_c$  from models.

We have estimated  $V_c$ ,  $D_c$  and  $V_{c, \text{pec}}$  values using the Table I data on radial velocities and distances of galaxies. The mean values for galaxies being located inside the virial core of the cluster, as well as for those residing within the  $R_0$  sphere, are presented in the lower part of the Table IV. In doing so we have considered Virgo members with accurate and supplement distances separately. The difference between the obtained values is within the statistical error. Our  $V_c$  estimates were corrected by  $+40 \text{ km s}^{-1}$  for restriction of velocity range:  $V_{\text{LG}} < 2000 \text{ km s}^{-1}$  with Virgo members velocity dispersion of  $600 \text{ km s}^{-1}$ . The following values:  $V_c = 984 \text{ km s}^{-1}$ ,  $D_c = 16.65$  Mpc and  $V_{c, \text{pec}} = -231 \text{ km s}^{-1}$  have been adopted as optimal parameters.

The number of galaxies with accurate velocities laying behind the Virgo cluster is small. The linear distance error for background galax-

ies with TF distances amounts up to 4–8 Mpc being comparable with  $R_0$ . That is why foreground galaxies with accurate distances remain the main source of data to probe the virgocentric infall. The distribution of these galaxies projected onto the Local Supercluster plane in Cartesian supergalactic coordinates is presented in Fig. 12. The arc of the circle denotes the zero-velocity surface with radius  $R_0$  and center located at  $SGX = -3.7$  Mpc,  $SGY = 16.1$  Mpc. The individual peculiar velocities of galaxies are smoothed by a Gaussian filter with  $\sigma = 0.75$  Mpc, and the resulting peculiar velocity field is outlined by level curves (in  $\text{km s}^{-1}$ ). Locations of three nearby groups: M 83, NGC 4244 and NGC 4258 are marked by ellipses.

As it can be seen, the zone of maximum positive velocities has an irregular shape rather elongated in the direction toward the center of the Local Supercluster. The infall velocity reaches approximately  $500 \text{ km s}^{-1}$ . The amplitude decrease with angular distance from the Virgo center due to the projection effects being lost among unknown possible variations in tangential motions.

We have selected galaxies with accurate distances and appropriate aspect:  $\lambda = [0-45^\circ]$  and  $\lambda = [135-180^\circ]$ , where  $\lambda$  is the angle between the line of sight and the vector connecting the cluster center with the position of a galaxy. The Hubble diagram based on the selected data is shown in Fig. 13. The top and the bottom panels correspond to the minor attractor and major attractor models. Galaxies located in front of the cluster and behind the cluster are marked with solid and open circles, respectively. Besides them, we have plotted the centers of groups with accurate mean distances and  $\lambda$  satisfying the condition above as squares. The central zone  $D_{vc} < 3.5$  Mpc omitted from the analysis of peculiar velocities is obscured. The direct/reverse regression lines for perturbed Hubble flow intersect the zero velocity level at 6.52 and 7.00 Mpc (minor attractor) and 6.97 and 7.49 Mpc (major attractor).

We have adopted  $R_0 = (7.0 \pm 0.3)$  Mpc as the mean estimate for the radius of the Virgo zero-velocity surface, and the corresponding value of  $M_T = (7.4 \pm 0.9) \times 10^{14} M_\odot$  for

the total mass of the cluster. This value is consistent with virial mass estimates for the Virgo Cluster:  $(7.5 \pm 1.5 \times 10^{14} M_\odot)$  [39] and  $7.0 \times 10^{14} M_\odot$  [42], corrected for the Hubble parameter  $H_0 = 73 \text{ km s}^{-1} \text{ Mpc}^{-1}$ . The remarkable agreement between the Virgo mass estimates based on internal (virial) and external motions of galaxies indicates that the cluster peripheral regions between  $R_V \simeq 2$  Mpc and  $R_0 \simeq 7$  Mpc do not contain a large amount of dark matter.

## CONCLUDING REMARKS

We have considered a sky region of  $100^\circ \times 20^\circ$  stretched along the Local Supercluster equator and centered at M 87 being known as the core of the Virgo cluster. This area occupies only 5% of the whole sky and contains 2158 galaxies with radial velocities  $V_{LG} < 2000 \text{ km s}^{-1}$ , which is about 40% of the total number of galaxies limited by velocity with  $2000 \text{ km s}^{-1}$ . We have determined Tully–Fisher distances  $D$  for 567 galaxies from our sample. Using literature data on distance estimates, the resulting ratio of LSC belt galaxies with peculiar velocities  $V_{pec} = V_{LG} - 73D$  amounts to 52%. The virial core of the Virgo cluster and the infall zone are well represented in the considered region, as well as the vast field areas.

The distribution of early type galaxies (E, S0) shows the well-known concentration toward the core of the Virgo cluster. The late type galaxies (S, I, BCD) are mostly presented beyond the virial radius. Gas-rich dwarf galaxies do not demonstrate any notable concentration toward the cluster.

Among 50 galaxy groups in the LSC belt, 6 groups have mean peculiar velocities  $500-1000 \text{ km s}^{-1}$  comparable with virial velocity dispersion of the Virgo galaxies. The cloud consisting of 20–30 galaxies around NGC 4278 (Coma I) is located at about 16 Mpc away from us and about 5 Mpc from the Virgo center, moving toward an observer with a velocity of  $840 \text{ km s}^{-1}$ . The nature of such an anomaly is not clear and requires the most careful consideration.

Galaxies in the vicinity of the Virgo cluster are involved in the virgocentric infall with an

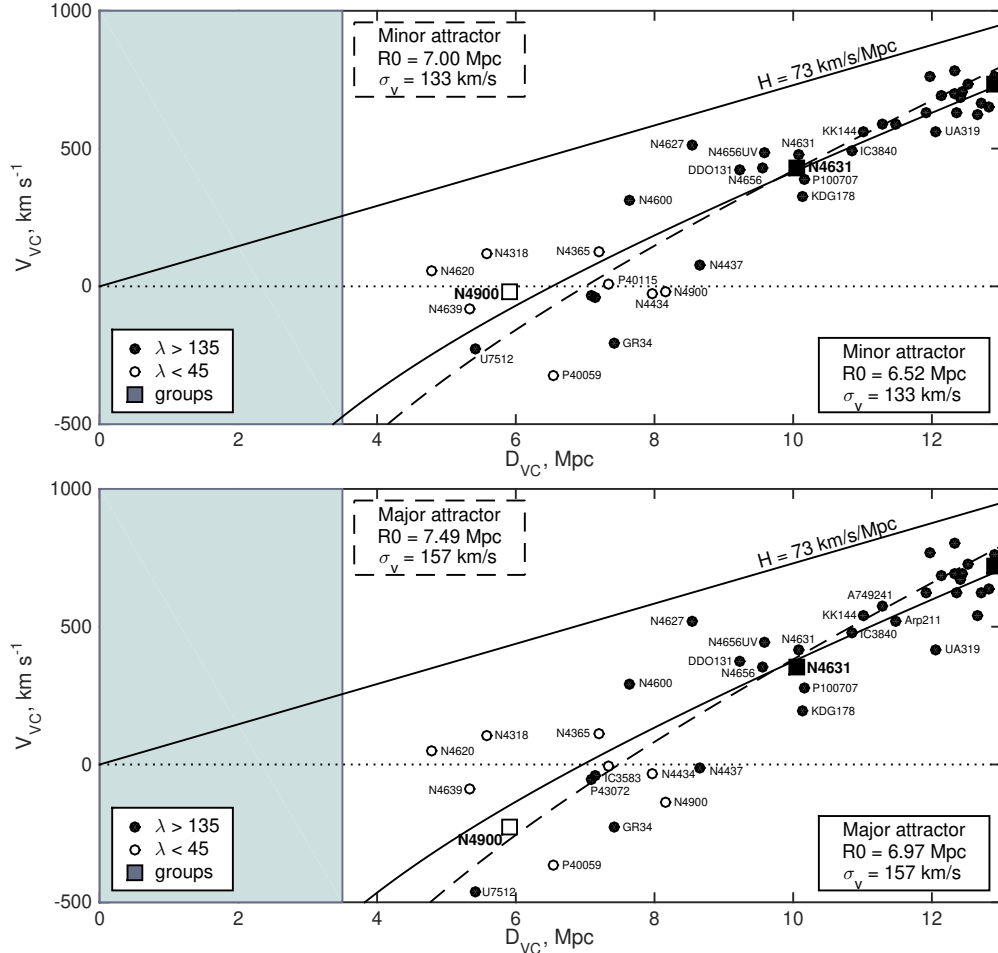


FIG. 13. Hubble diagram: velocity vs. distance relative to the center of the Virgo cluster. Top and bottom panel correspond to the minor attractor and major attractor models. The central zone omitted from the analysis of peculiar velocities is denoted with grey. Individual galaxies are marked by circles, galaxy groups—by squares. Solid and open symbols stay for galaxies located in front and behind the cluster, respectively.

amplitude of about  $500 \text{ km s}^{-1}$ . Based on accurately measured distances, we have estimated the radius of the zero-velocity surface for the Virgo cluster to be  $R_0 = (7.0 \pm 0.3) \text{ Mpc}$ . This value corresponds to the total mass of the cluster  $M_T = (7.4 \pm 0.9) \times 10^{14} M_\odot$  in good agreement with its virial mass estimate. Such an agreement indicates that the peripheral regions of the Virgo cluster within nearly  $4R_V$  do not contain a significant amount of dark matter. The similar result was obtained for the Local Group and other neighboring groups [25].

While preparing this paper, we have become aware of the work of Shaya et al. [49] on the dynamics of the Local Supercluster in which the

authors give the Virgo  $R_0$  and  $M_T$  estimates for the Virgo cluster consistent with our results within statistical errors.

The authors are grateful to the Russian Science Foundation (RSF grant No. 14-12-00965). The authors acknowledge the usage of the HyperLeda (<http://leda.univ-lyon1.fr>) and NED (<http://ned.ipac.caltech.edu>) databases. The authors thank Dmitry Makarov for his useful comments.

- [1] A. Klypin, Y. Hoffman, A. V. Kravtsov, and S. Gottlöber, *Astrophys. J.* **596**, 19 (2003).

- [2] W. E. Schaap, Ph.D. Thesis (University of Groningen, 2007).
- [3] L. Ceccarelli, A. N. Ruiz, M. Lares, et al., *Monthly Notices Royal Astron. Soc.* **461**, 4013 (2016).
- [4] A. Kogut, C. Lineweaver, G. F. Smoot, et al., *Astrophys. J.* **419**, 1 (1993).
- [5] R. B. Tully, E. J. Shaya, I. D. Karachentsev, et al., *Astrophys. J.* **676**, 184-205 (2008).
- [6] R. B. Tully, H. M. Courtois, and J. G. Sorce, *Astron. J.* **152**, 50 (2016).
- [7] R. Scaramella, *Astrophys. Lett. Commun.* **32**, 137 (1995).
- [8] R. C. Kraan-Korteweg, *Astron. and Astrophys. Suppl.* **66**, 255 (1986).
- [9] K. L. Masters, Ph.D. Thesis (Cornell University, New York, USA, 2005).
- [10] B. S. Koribalski, L. Staveley-Smith, V. A. Kilborn, et al., *Astron. J.* **128**, 16 (2004).
- [11] M. P. Haynes, R. Giovanelli, A. M. Martin, et al., *Astron. J.* **142**, 170 (2011).
- [12] K. Kovač, T. A. Oosterloo, and J. M. van der Hulst, *Monthly Notices Royal Astron. Soc.* **400**, 743 (2009).
- [13] R. B. Tully and J. R. Fisher, *Astron. and Astrophys.* **54**, 661 (1977).
- [14] S. Mei, J. P. Blakeslee, P. Côté, et al., *Astrophys. J.* **655**, 144 (2007).
- [15] I. D. Karachentsev, O. G. Nasonova, and H. M. Courtois, *Astrophys. J.* **743**, 123 (2011).
- [16] I. D. Karachentsev, O. G. Nasonova, and H. M. Courtois, *Monthly Notices Royal Astron. Soc.* **429**, 2264 (2013).
- [17] I. D. Karachentsev and O. G. Nasonova, *Monthly Notices Royal Astron. Soc.* **429**, 2677 (2013).
- [18] I. D. Karachentsev, O. G. Nasonova, and V. E. Karachentseva, *Astrophysical Bulletin* **70**, 1 (2015).
- [19] I. D. Karachentsev, V. E. Karachentseva, and O. G. Nasonova, *Astrophysics* **57**, 457 (2014).
- [20] I. D. Karachentsev, O. G. Kashibadze, and V. E. Karachentseva, *Astrophysical Bulletin* **72**, 111 (2017).
- [21] I. D. Karachentsev and O. G. Nasonova, *Monthly Notices Royal Astron. Soc.* **405**, 1075 (2010).
- [22] O. G. Nasonova, J. A. de Freitas Pacheco, and I. D. Karachentsev, *Astron. and Astrophys.* **532**, A104 (2011).
- [23] O. G. Nasonova and I. D. Karachentsev, *Astrophysics* **54**, 1 (2011).
- [24] D. Makarov, P. Prugniel, N. Terekhova, et al., *Astron. and Astrophys.* **570**, A13 (2014).
- [25] O. G. Kashibadze and I. D. Karachentsev, *Astron. and Astrophys.* **609**, A11 (2018).
- [26] K. N. Abazajian, J. K. Adelman-McCarthy, M. A. Agüeros, et al., *Astrophys. J.s* **182**, 543-558 (2009).
- [27] K. C. Chambers, E. A. Magnier, N. Metcalfe, et al., arXiv:1612.05560 (2016).
- [28] R. B. Tully and M. J. Pierce, *Astrophys. J.* **533**, 744 (2000).
- [29] I. D. Karachentsev, E. I. Kaisina, and O. G. Kashibadze, *Astron. J.* **153**, 6 (2017).
- [30] M. G. Lee, W. L. Freedman, and B. F. Madore, *Astrophys. J.* **417**, 553 (1993).
- [31] J. L. Tonry, A. Dressler, J. P. Blakeslee, et al., *Astrophys. J.* **546**, 681 (2001).
- [32] L. Ferrarese, P. Côté, J.-C. Cuillandre, et al., *Astrophys. J.s* **200**, 4 (2012).
- [33] M. P. Haynes, R. Giovanelli, and G. L. Chincharini, *Annual Rev. Astron. Astrophys.* **22**, 445 (1984).
- [34] P. A. R. Ade et al. (Planck Collab), *Astron. and Astrophys.* **596**, A101 (2016).
- [35] D. Makarov and I. Karachentsev, *Monthly Notices Royal Astron. Soc.* **412**, 2498 (2011).
- [36] G. L. Hoffman, D. W. Olson, and E. E. Salpeter, *Astrophys. J.* **242**, 861 (1980).
- [37] J. L. Tonry and M. Davis, *Astrophys. J.* **246**, 680 (1981).
- [38] G. L. Hoffman and E. E. Salpeter, *Astrophys. J.* **263**, 485 (1982).
- [39] R. B. Tully and E. J. Shaya, *Astrophys. J.* **281**, 31 (1984).
- [40] P. Teerikorpi, L. Bottinelli, L. Gouguenheim, and G. Paturel, *Astron. and Astrophys.* **260**, 17 (1992).
- [41] T. Ekholm, P. Lanoix, P. Teerikorpi, et al., *Astron. and Astrophys.* **351**, 827 (1999).
- [42] J. L. Tonry, J. P. Blakeslee, E. A. Ajhar, and A. Dressler, *Astrophys. J.* **530**, 625 (2000).
- [43] I. D. Karachentsev, R. B. Tully, P.-F. Wu, et al., *Astrophys. J.* **782**, 4 (2014).
- [44] G. de Vaucouleurs, *Astrophys. J.* **131**, 585 (1960).
- [45] E. Giraud, *Astrophys. J.l* **524**, L15 (1999).
- [46] B. Binggeli, C. C. Popescu, and G. A. Tammann, *Astron. and Astrophys. Suppl.* **98**, 275 (1993).
- [47] E. Kourkchi and R. B. Tully, *Astrophys. J.* **843**, 16 (2017).
- [48] S. Kim, S.-C. Rey, H. Jerjen, et al., *Astrophys. J.s* **215**, 22 (2014).
- [49] E. J. Shaya, R. B. Tully, Y. Hoffman, and D. Pomarède, *Astrophys. J.* **850**, 207 (2017).

TABLE I. Galaxies in the Local Supercluster band

Name	RA(J2000.0)	Dec	SGL SGB	$V_{LG}$	type	$B_T$	$W_{50}$	$m_{21}$	$m - M$	$D$	meth
			deg	km/s		mag	km/s	mag	mag	Mpc	
(1)	(2)	(3)	(4)	(5)	(6)	(7)	(8)	(9)	(10)	(11)	
UGC05460	100809.2+515040	54.42-10.53	1146	Sd	13.88	93	14.87	31.23	17.80	tf	
UGC05459	100810.1+530501	53.50-09.68	1170	Scd	13.19	274	13.61	31.56	20.50	tf	
PGC2427800	101306.5+525646	54.11-09.23	1545	BCD	17.40	-	-	-	-	-	
SDSSJ101540.57+523202.4	101540.6+523202	54.69-09.21	1206	I	18.15	37	18.40	31.27	17.99	TF	
UGC05571	101942.4+520356	55.46-09.06	724	Im	16.45	51	15.34	29.58	8.24	TFb	
SDSSJ102225.42+475218.3	102225.5+475218	59.01-11.42	1650	Sm	18.14	-	-	-	-	-	
PGC030715	102701.8+561614	52.90-05.53	914	BCD	16.08	58	16.24	30.18	10.84	TF	
UGC05676	102904.9+544301	54.30-06.29	1499	Sdm	14.81	123	16.05	31.72	22.08	TF	
PGC2381991	103108.9+504709	57.60-08.49	983	Sm	16.58	-	-	-	-	-	
NGC3264	103219.6+560502	53.51-05.08	1010	Sd	12.61	143	14.47	31.40	19.43	tf	
UGC05720	103231.9+542404	54.86-06.09	1510	BCD	13.16	142	15.92	31.50	20.00	TF	
UGC05740	103445.9+504606	57.97-08.05	698	Sm	15.59	138	14.91	32.29	28.73	TFb	
PGC2277751	103512.1+461412	61.68-10.71	530	BCD	17.46	-	-	-	-	-	
PGC2368186	103559.8+501631	58.48-08.19	896	I	17.64	-	-	-	-	-	
PGC2302764	103625.0+474153	60.62-09.67	1590	BCD	18.08	86	17.10	32.76	35.6	TFb	
PGC2425292	103636.3+525101	56.47-06.56	1043	BCD	16.08	124	16.31	32.66	34.1	TF	
PGC2302994	103825.7+474236	60.81-09.39	1611	BCD	16.73	69	16.59	31.78	22.70	TF	
NGC3310	103845.9+533012	56.14-05.91	1055	Sbc	11.28	190	13.29	-	-	-	
UGC05791	103926.9+475650	60.72-09.12	890	Sbc	14.50	157	15.98	32.11	26.40	tf	
UGC05798	103947.1+475557	60.76-09.08	1574	Scd	14.45	184	15.76	32.54	32.30	tf	
SDSSJ103950.97+564402.9	103951.3+564401	53.63-03.85	1216	Sm	16.90	-	-	-	-	-	
PGC2336386	104042.4+491224	59.81-08.21	1544	Im	17.10	117	16.20	32.72	34.9	TFb	
PGC031888	104214.2+474600	61.14-08.84	1562	S0	15.29	-	-	-	-	-	
PGC2362930	104251.9+500619	59.28-07.40	1670	BCD	16.94	-	-	-	-	-	
SDSSJ104407.79+474242.1	104407.8+474242	61.37-08.61	1570	BCD	17.63	-	-	-	-	-	
UGC05848	104423.1+562517	54.25-03.53	902	Sm	15.14	133	15.41	31.98	24.9	TF	
KKH062	104455.7+541225	56.11-04.76	1070	I	18.2	41	17.11	30.66	13.55	TFb	
NGC3353	104522.4+555737	54.71-03.69	1020	Sb	13.22	90	14.94	31.42	19.30	tf	
UGC05883	104719.3+540216	56.45-04.57	844	Im	15.51	65	15.62	30.45	12.30	TF	
UGC05888	104745.7+560529	54.80-03.34	1319	Im	15.19	104	15.34	31.59	20.78	TF	
PGC2288707	104747.1+465246	62.42-08.58	1521	Sd	17.99	-	-	-	-	-	
UGC05917	104853.8+464315	62.66-08.51	768	Sm	15.17	98	15.75	31.10	16.60	TF	
SDSSJ105107.83+512013.3	105107.8+512013	59.01-05.62	862	I	18.24	-	-	-	-	-	
UGC05953	105118.1+443419	64.71-09.34	1819	S0	13.34	-	-	-	-	-	
PGC2457837	105129.6+540205	56.80-04.07	1400	I	16.59	-	-	-	-	-	
PGC2554441	105132.9+570027	54.34-02.39	1950	Scd	16.82	-	-	-	-	-	
UGC05976	105202.8+553604	55.54-03.12	1289	Sdm	15.12	93	15.35	-	-	-	
UGC05996	105257.4+402242	68.47-11.35	1627	Sd	16.44	60	15.16	31.04	16.14	TFb	
UGC05998	105308.4+501705	60.07-05.94	1437	Sm	14.74	173	15.82	32.34	29.44	TF	
UGC06005	105327.7+460111	63.69-08.24	748	Sd	16.80	-	-	-	-	-	
UGC06016	105412.8+541714	56.81-03.60	1583	Im	16.10	139	14.60	32.00	25.11	TFb	
NGC3448	105439.4+541818	56.83-03.53	1443	Sb	12.41	258	12.85	31.33	18.45	TF	
UGC06029	105502.3+494334	60.71-05.99	1418	I	14.19	153	14.78	31.85	23.4	TF	
PGC2389897	105508.2+511119	59.48-05.18	1423	BCD	17.73	-	-	-	-	-	
NGC3458	105601.5+570701	54.58-01.83	1856	S0	13.05	-	-	-	-	-	
UGC06041	105617.5+413603	67.75-10.17	1472	Sd	16.95	95	16.54	32.57	32.7	TFb	
UGC06039	105620.9+564535	54.91-01.99	1932	Scd	16.23	-	-	-	-	-	
PGC032915	105658.7+500826	60.53-05.51	1427	BCD	17.20	63	16.33	31.08	16.44	TFb	
PGC2351264	105849.6+494258	61.05-05.48	880	BCD	16.79	-	-	-	-	-	
PGC033085	105918.9+423523	67.19-09.18	1567	BCD	17.34	-	-	-	-	-	
PGC033137	110000.2+542532	57.15-02.81	1077	Sdm	16.79	39	16.41	30.46	12.34	TFb	



TABLE II. List of 50 MK-groups within the LSC band

Group	SGL	SGB	$N_v$	$\langle V_{LG} \rangle$	$D$	$V_{pec}$
	deg	deg		km/s	Mpc	km/s
(1)	(2)	(3)	(4)	(5)	(6)	(7)
NGC3458	54.59	-1.83	6	2000	-	-
NGC3610	54.68	1.57	19	1794	28.3	-272
NGC3665	72.93	-6.81	11	2038	30.8	-210
NGC3769	65.71	-0.73	6	780	15.1	-322
NGC3838	56.91	4.25	11	1368	29.0	-749
NGC3877	66.64	0.40	21	955	16.4	-242
NGC3900	85.83	-6.90	4	1745	31.0	-518
NGC3992	61.87	4.30	72	1097	18.5	-253
NGC4062	82.41	-2.13	4	736	14.5	-322
NGC4111	72.11	2.22	20	851	16.8	-375
NGC4123	110.43	-10.46	5	1150	16.9	-84
NGC4151	75.78	1.63	16	1031	14.7	-42
NGC4150	84.29	-1.32	4	211	16.2	-972
NGC4157	65.30	5.29	8	834	17.5	-443
NGC4189	100.66	-6.01	6	1987	30.0	-203
NGC4217	68.78	4.98	5	1085	19.1	-309
NGC4216	101.08	-5.60	16	55	-	-
NGC4244	77.73	2.41	8	291	4.3	-23
NGC4258	68.74	5.55	15	551	7.7	-11
NGC4261	108.38	-6.94	87	2060	29.4	-86
NGC4274	85.67	0.34	14	990	16.3	-200
NGC4303	109.86	-6.72	23	1387	-	-
NGC4321	99.03	-3.18	17	1515	-	-
NGC4346	69.26	6.19	5	787	16.4	-410
NGC4342	107.50	-5.57	5	596	-	-
NGC4402	101.86	-3.24	4	117	-	-
NGC4472	107.02	-3.85	355	992	16.5	-212
NGC4490	74.79	5.94	8	583	8.9	-67
NGC4527	112.47	-4.30	18	1592	14.5	534
NGC4535	107.15	-2.71	23	1747	-	-
NGC4546	118.80	-5.72	4	879	11.9	10
NGC4552	103.06	-1.17	12	230	-	-
NGC4565	90.21	2.76	11	1191	14.0	169
NGC4594	126.69	-6.68	11	856	9.6	155
NGC4631	84.22	5.74	28	635	7.4	95
NGC4636	113.03	-2.20	32	757	17.8	-542
NGC4643	113.75	-2.27	9	1195	-	-
NGC4666	116.23	-2.50	16	1427	16.7	208
NGC4697	121.60	-3.11	37	1175	14.9	87
NGC4753	117.43	-0.96	23	992	19.7	-446
NGC4808	112.36	1.36	5	591	-	-
NGC4856	131.23	-3.02	5	1189	19.4	-227
NGC4866	103.07	4.84	5	1909	30.1	-288
NGC4900	114.42	2.03	8	779	21.0	-754
NGC4995	124.98	1.38	4	1569	21.3	14
NGC5054	133.93	0.61	7	1556	-	-
NGC5078	144.44	-1.85	26	1849	26.7	-100
NGC5084	139.13	-0.13	12	1560	22.4	-75
NGC5170	136.11	3.15	4	1313	-	-
NGC5236	147.93	0.99	12	321	4.9	-37

TABLE III. Galaxies around NGC 4278 with high peculiar velocities and some other probable companions to NGC 4278

Name	RA (2000.0)	Dec	T	$V_{LG}$	$D$	meth	$B_T$	$V_{pec}$
(1)	(2)	(3)	(4)	(5)	(6)	(7)	(8)	(8)
			km/s	Mpc		mag	km/s	
DDO97	114857.2+235016	10	452	13.7	bs	15.1	-548	
UGC6881	115444.7+200320	10	522	16.4	TF	15.8	-675	
PGC4561602	115504.2+282053	-2	458	-	-	17.8	-	
AGC731823	115522.5+282030	9	512	23.8	TF	16.4	-1225	
KDG82	115539.4+313110	8	558	16.6	TF	14.8	-654	
BTS76	115844.1+273506	10	407	15.	rgb	16.5	-688	
KUG1157+31	120016.2+311330	8	582	14.8	TF	15.1	-498	
NGC4080	120451.8+265933	8	517	15.0	TF	13.7	-578	
LV1205+28	120534.2+281355	8	462	19.5	TF	16.7	-962	
PGC4560429	120633.5+303716	-2	464	-	-	18.2	-	
UGC7131	120911.8+305424	8	224	16.8	TF	15.7	-1002	
NGC4150	121033.6+302406	-1	210	13.7	sbf	12.5	-790	
KK127	121322.7+295518	9	103	17.3	TF	15.6	-1160	
AGC732009	121348.4+295731	10	196	16.5	TF	17.4	-1008	
LV1217+32	121732.0+323157	9	433	15.	rgb	18.4	-662	
UGC7321	121734.0+223225	7	339	17.2	TF	14.1	-917	
AGC229053	121815.5+253406	10	376	17.9	TF	17.9	-931	
KKH07J1218+30	121831.5+300340	10	600	-	-	17.0	-	
BTS116	121857.3+283311	-3	289	-	-	16.2	-	
IC 779	121938.7+295300	-1	187	16.7	sbf	15.2	-1032	
PGC0213976	121943.6+293932	-2	549	-	-	17.3	-	
NGC4278	122006.8+291651	-2	588	16.1	sbf	11.1	-587	
NGC4286	122042.1+292045	2	611	14.7	TF	14.5	-448	
PGC1853813	122116.6+290221	-2	588	-	-	16.5	-	
NGC4308	122156.9+300427	-1	612	-	-	14.1	-	
PGC4323538	122216.7+305324	-1	545	-	-	17.1	-	
UGC07438	122219.5+300341	6	678	22.3	TF	15.8	-950	
PGC040195	122309.7+292059	-2	524	-	-	15.6	-	
IC 3247	122314.0+285338	7	546	24.4	TF	15.4	-1235	
AGC749235	122409.9+261352	10	246	-	-	19.8	-	
IC 3308	122517.9+264253	8	277	12.8	TF	15.4	-657	
AGC749236	122542.4+264836	10	234	15.1	TFb	16.6	-868	
NGC4414	122627.1+311324	5	719	17.9	cep	11.0	-588	
NGC4448	122815.5+283713	2	659	23.8	tf	12.0	-1078	
UGC7699	123248.0+373718	7	514	14.5	TF	13.3	-544	
UGC7774	123622.5+400019	7	563	22.6	TF	14.6	-1087	
FGC1497	124700.6+323905	8	522	23.4	TF	16.8	-1186	
UGC7990	125027.2+282110	10	495	20.4	TF	16.2	-994	

TABLE IV. The mean radial velocity and mean distance of Virgo cluster

Sample	Number	$V_c(LG)$ km/s	$D_c$ Mpc	$V_{c,pec}$ km/s	Reference
All members (V)	385	$956 \pm 55$	[16.5]	-248	Binggeli et al, 1993
Core members (V)	271	$935 \pm 35$	[16.5]	-270	Binggeli et al, 1993
All members (D)	79	$1034 \pm 61$	$16.5 \pm 0.1$	-170	Mei et al, 2007
Core members (D)	32	$984 \pm 105$	$16.7 \pm 0.2$	-235	Mei et al, 2007
Infall pattern	189	-	-	-139	Tonry et al, 2000
Cosmic flow	-	-	-	-185	Tully et al, 2008
Within $R_v$ , accur	75	$950 \pm 62$	$16.45 \pm 0.08$	-251	present paper
Within $R_0$ , accur	119	$975 \pm 46$	$16.32 \pm 0.16$	-216	present paper
Within $R_0$ , suppl	372	$996 \pm 27$	$16.44 \pm 0.16$	-204	present paper
Within $R_0$ , all	491	$985 \pm 23$	$16.38 \pm 0.14$	-211	present paper
Adopted		984	16.65	-231	